ENVIRONMENTAL RESEARCH

LETTERS

LETTER • OPEN ACCESS

Exposure to cold temperature affects the spring phenology of Alaskan deciduous vegetation types

To cite this article: Mingjie Shi et al 2020 Environ. Res. Lett. 15 025006

View the <u>article online</u> for updates and enhancements.

Environmental Research Letters



OPEN ACCESS

RECEIVED

24 January 2019

REVISED

19 December 2019

ACCEPTED FOR PUBLICATION

23 December 2019

PUBLISHED

7 February 2020

Original content from this work may be used under the terms of the Creative Commons Attribution 4.0 licence.

Any further distribution of this work must maintain attribution to the author(s) and the title of the work, journal citation and DOI



LETTER

Exposure to cold temperature affects the spring phenology of Alaskan deciduous vegetation types

Mingjie Shi^{1,2,7}, Nicholas C Parazoo¹, Su-Jong Jeong³, Leah Birch⁴, Peter Lawrence⁵, Eugenie S Euskirchen⁶ and Charles E Miller¹

- 1 Jet Propulsion Laboratory, California Institute of Technology, 4800 Oak Grove Drive, Pasadena, CA 91109, United States of America
- ² Joint Institute for Regional Earth System Science and Engineering, University of California at Los Angeles, Los Angeles, CA 90095, United States of America
- 3 Department of Environmental Planning, Graduate School of Environmental Studies, Seoul National University, Seoul, Republic of Korea
- ⁴ Woods Hole Research Center, Falmouth, MA 02540, United States of America
- ⁵ National Center for Atmospheric Research, Boulder, CO 80305, United States of America
- ⁶ University of Alaska Fairbanks, Institute of Arctic Biology, Fairbanks, AK 99775, United States of America
- Author to whom any correspondence should be addressed.

E-mail: mingjie.shi@jpl.nasa.gov

Keywords: Alaskan deciduous vegetation, leaf budburst, GPP onset, community land model, chilling requirement Supplementary material for this article is available online

Abstract

Temperature is a dominant factor driving arctic and boreal ecosystem phenology, including leaf budburst and gross primary production (GPP) onset in Alaskan spring. Previous studies hypothesized that both accumulated growing degree day (GDD) and cold temperature (chilling) exposure are important to leaf budburst. We test this hypothesis by combining both satellite and aircraft vegetation measurements with the Community Land Model Version 4.5 (CLM), in which the end of plant dormancy depends on thermal conditions (i.e. GDD). We study the sensitivity of GPP onset of different Alaskan deciduous vegetation types to a GDD model with chilling requirement (GC model) included. The default CLM simulations have a 1-12 d earlier day of year GPP onset over Alaska vegetated regions compared to satellite constrained estimates from the Polar Vegetation Photosynthesis and Respiration Model. Integrating a GC model into CLM shifts the phase and amplitude of GPP. During 2007–2016, mean GPP onset is postponed by $5\pm7,4\pm8$, and 1 ± 6 d over Alaskan northern tundra, shrub, and forest, respectively. The GC model has the greatest impact during warm springs, which is critical for predicting phenology response to future warming. Overall, spring GPP high bias is reduced by 10%. Thus, including chilling requirement in thermal forcing models improves northern high-latitude phenology, but leads to other impacts during the growing season which require further investigation.

1. Introduction

Vegetation phenology is crucial to the dynamic response of terrestrial ecosystems to climate change (Euskirchen *et al* 2014), since vegetation affects surface radiation, temperature, energy exchange, the hydrological cycle, and the carbon cycle (Myneni *et al* 1997, Schaefer *et al* 2005, Euskirchen *et al* 2006, Piao *et al* 2007, Bonan 2008, Sitch *et al* 2008, Jeong *et al* 2011, Euskirchen *et al* 2014). A better understanding and prediction of ecosystem phenology is essential for

reducing uncertainties in modeling carbon, water, and energy cycles, and their feedback to climate (Levis and Bonan 2004). The model comparison of the North American Carbon Program model intercomparison suggests that compared to observations, most terrestrial biosphere models (TBMs) simulate earlier starts (i.e. typically two weeks) of the growing season in deciduous forests, and the predicted leaf onset dates under different climate scenarios are highly uncertain as a result of the dependence of predicted response to warming on model structures (Richardson *et al* 2012).

Further, early starts of the growing season could be the reason for the over-estimation of gross ecosystem photosynthesis during the spring transition in TBMs (Richardson *et al* 2012). Thus, accurate simulation of vegetation phenology remains a major challenge in TBMs.

In most TBMs, leaf onset of deciduous types could be triggered in different ways: temperature threshold (El Maayar et al 2002), growing degree day (GDD; Sitch et al 2003), GDD and radiation accumulation (Thornton et al 2002), and GDD and chilling requirement (Krinner et al 2005). Here, GDD refers to the accumulated mean surface air temperature above a given threshold (e.g. 0 °C). Studies have shown that some temperate and boreal deciduous tree species need the exposure to certain ranges of cold temperature (i.e. chilling requirement) to break dormancy (Baldocchi and Wong 2008, Schwartz and Hanes 2010, Delpierre et al 2016). Here, the chilling requirement is species-specific (Laube et al 2014); for example, the number of chill days (with daily mean surface air temperature less than 5 °C) before the break of dormancy is ~100 for temperate deciduous trees (Jeong et al 2012). Modeling based studies also support that the chilling requirement is essential to deciduous species for the break of dormancy, regulating the timing of leaf budburst (White et al 1997, Krinner et al 2005, Jeong et al 2012, Richardson et al 2012, Clark et al 2014). Thus, there have been several efforts to move beyond a simple thermal forcing model approach (GDD models; White et al 1997, Sitch et al 2003) and test more sophisticated GDD models that account for chilling period (herein GC model; Krinner et al 2005, Caffarra et al 2011, Jeong et al 2012). For example, Jeong et al (2012) find that using a chilling model shifts the zero-crossing date for net carbon uptake by ~ 11 d in temperate deciduous trees. Additionally, Richardson and O'Keefe (2009) show that the GC models are the best for 20 of 33 species, while the GDD only models are the best for 13 of 33 species at Harvard forest. Chiang and Brown (2007) also show that the phenology simulations from a three-parameter GC model suite the observations for all 17 selected species at Harvard forest. Thus, thorough tests of budburst models, including and excluding the chilling requirement, demonstrate that GC models work well for broadleaf deciduous temperate species.

Previous GC model comparisons (e.g. Richardson et al 2012) and sensitivity experiments (e.g. Jeong et al 2012) have mostly focused on deciduous plants in temperate regions, with less attention to temperature limited high latitude ecosystems. The Arctic has experienced severe changes, mainly characterized by an amplification of surface air temperature (Serreze et al 2009, Screen and Simmonds 2010, Screen et al 2013), which is altering the phenology of Arctic vegetation, favoring earlier leaf-out and photosynthesis (Randerson et al 1999, Euskirchen et al 2006, Zeng et al 2011, Piao et al 2013, Melaas et al 2018). This study

explicitly investigates phenology modeling of Arctic deciduous types. It is suggested that the sensitivity of leaf budburst to accumulated growing degrees and chilling temperatures varies among different deciduous plant types in arctic tundra and boreal ecosystems (Euskirchen et al 2014, Delpierre et al 2016). In addition, post-snow melt air temperature is suggested as the dominant factor controlling leaf budburst and growth phenology in Arctic tundra and boreal ecosystems (Delbart and Picard 2007, Wipf and Rixen 2010). Delpierre et al (2016) also demonstrate that for a majority of boreal tree species, a certain duration of chilling is needed for the release from endodormancy, followed by leaf budburst. Thus, we hypothesize that all the Arctic deciduous species need certain exposure to cold temperature for budburst, which regulates the vegetation phenology and carbon fluxes. We focus our analysis on Alaska, where aircraft and in situ carbon flux observations are available for the GC model benchmark. The specific objectives of the study are to (1) estimate the sensitivity of leaf budburst and photosynthetic onset of varied Alaskan deciduous vegetation types (e.g. deciduous forest, deciduous shrub, and C3 arctic grass) to a GC model and (2) to estimate resulting changes in net carbon uptake associated with leaf budburst timing.

2. Method

2.1. Model experimental design

2.1.1. Terrestrial biosphere model

We use the Community Land model Version 4.5 (CLM4.5) BGC (Oleson *et al* 2013), which has prognostic carbon dynamics and is a land model option of the Community Earth System Model Version 1.2 (CESM1.2). In CLM, the phenology onset is based on an accumulated GDD approach (White $et\,al\,1997$), in which the onset GDD_{CLM} is defined as:

$$GDD(t)_{CLM} = \sum_{lan1}^{day} (T_{SOIL,3} > 0 \, ^{\circ}C), \tag{1}$$

where 'day' represents Julian day, and $T_{\rm SOIL,3}$ is the third soil layer (45–90 mm soil depth) temperature. The onset period is initiated if GDD_{CLM} is larger than a critical onset threshold calculated as:

GDD_{sum_crit} = exp (4.8 + 0.13(
$$T_{2 \text{ m,ann_avg}}$$
, (2)
- $T_{\text{freezing_point}}$))

where $T_{2 \text{ m,ann_avg}}$ is the annual mean of the 2 m air temperature (K) and $T_{\text{freezing_point}}$ is the freezing point of water (273.15 K; Oleson *et al* 2013). That is, the phenology in CLM starts when GDD_{CLM} exceeds GDD_{sum_crit}; thus, meeting a threshold (i.e. GDD_{sum_crit}) of accumulated heat for budburst.

2.1.2. The GC model integrated into CLM

We integrated the leaf budburst scheme parameterized by Jeong $et\ al\ (2012)$ into CLM. The scheme discussed



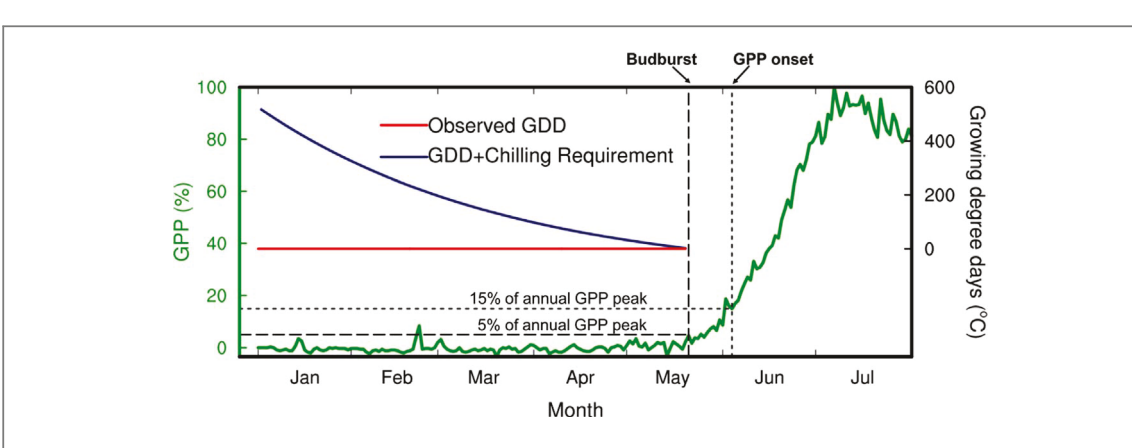


Figure 1. The diagram of GDD (the red line; equation (3)) and GDD plus chilling requirement (the navy line; GC threshold defined by the right side of equation (4)) regulated leaf budburst and GPP onset. The leaf budburst starts when GDD is larger than the GC threshold, and the red line and blue line cross at the budburst starting point. The GPP and surface air temperature ($T_{\rm AIR}$) data are obtained from site measurements at Imnavait Creek watershed (68.4 °N, 149.2 °W; Euskirchen *et al* 2016). GDD and GC threshold in equation (4) are calculated with the $T_{\rm AIR}$ data at this site. In this example, there is not a day with daily $T_{\rm AIR}$ higher than 5 °C when observed leaf budburst starts.

by Jeong *et al* (2012) assumes that leaf budburst has chilling requirement and chill days reduce the GDD requirement. Here, GDD is based on a thermal forcing model and defined as (Jeong *et al* 2012):

$$GDD(t) = \sum_{l=1}^{\text{day}} \max(T - 5 \, ^{\circ}\text{C}, \, 0), \quad (3)$$

where 'day' represents Julian day and *T* is surface air temperature. This scheme predicts that leaf budburst occurs when

GDD(t)
$$\geqslant a + b \times \exp[c \times \text{NCD}(t)]$$

+ $d(T_{\text{Ian-Feb}} + 5.5 \,^{\circ}\text{C}),$ (4)

where NCD is defined as the number of chill days (any day with daily mean surface air temperature (T_{AIR}) less than 5 °C constitutes a chill day) and T_{Jan-Feb} is daily mean T_{AIR} (°C) averaged over January and February (Jeong et al 2013). We define the right side of equation (4) as the GC threshold (figure 1). Here, a, b, c, and d are adjustable parameters (table S1 is available online at stacks.iop.org/ERL/15/025006/mmedia). We find that the ranges of a, b, and c developed in Jeong et al (2012) can well represent temperate deciduous forest spring phenology but some of the parameter groups cannot accurately represent the spring phenology in Alaska. Thus, we re-evaluate the adjustable parameters in Jeong et al (2012) and select two sets of coefficients (i.e. expl and exp2) that reasonably represent the spring phenology of Alaskan deciduous vegetation, as listed in table S1. Leaf growth phenology of tundra in North Slope Alaska is postponed more by exp2 than by exp1 (figure not shown; text S1). Thus, we design the third experiment by applying the parameters of exp1 to broadleaf deciduous shrub, which is the dominant vegetation type over North Slope Alaska as suggested by CLM plant functional type (PFT) maps (section 2.1.3), and applying the parameters of exp2 to broadleaf deciduous boreal tree type and C3 arctic grass (figure S1). This experiment is denoted exp3 (table S1).

2.1.3. The surface vegetation map of CLM

The PFT map in CLM is developed by using moderate resolution imaging spectroradiometer (MODIS) land surface mapping (Lawrence and Chase 2007). In Alaska, the vegetation cover fraction for needleleaf evergreen tree, broadleaf deciduous tree, broadleaf deciduous shrub, and C3 arctic grass is 21.2%, 3.6%, 36.5%, and 19.1%, respectively (table S2). We acknowledge that mapping the vegetation communities over the pan-Arctic and applying them to TBMs remain a challenge. Compared to the current CLM PFT map, a more diverse vegetation functional classification, such as a species-group based classification (Euskirchen et al 2014), is needed but beyond the scope of this study. Further, vegetation mapping over tundra, such as the North Slope Alaska, is more uncertain (Berner et al 2018). Nevertheless, the CLM PFT map prescribes shrubland over North Slope Alaska representing low-lying shrubs, consistent with satellite-observation and regression-algorithm based shrub maps (Beck et al 2011, Berner et al 2018), in which low-lying wetland areas on the coastal plain of the North Slope have the lowest shrub cover and ~50% of the North Slope areas have shrub cover fraction $\geq 50\%$ (figure S1).

2.1.4. Model setups

We use the atmospheric forcing data of Climatic Research Unit-National Centers for Environmental Prediction Version 7 (CRUNCEP7) at $0.5^{\circ} \times 0.5^{\circ}$ spatial resolution as the forcing data of CLM (Lawrence *et al* 2019). Our primary analysis, which focuses on the sensitivity of leaf budburst and photosynthetic onset to GDD and chilling requirement, uses the default CLM and CLM with the GC model integrated (i.e. CLM_GC) driven by CRUNCEP7 and the surface PFT map from CESM1.2. Here, CLM and CLM_GC are run at the 0.9° latitude $\times 1.25^{\circ}$ longitude and 30 min spatiotemporal resolution during 2007–2016,



Table 1. CLM used forcing data and surface data.

Meteorological forcing	Surface PFT data	Name of the experiments		
Toronig	777 uuu	Default model	CLM with GC integrated	
CRUNCEP7	CESM1.2	CLM	CLM_GCexp1 ^a CLM_GCexp2 ^a CLM_GCexp3 ^a	

^a The parameters of the experiments are included in table S1.

when both CRUNCEP7 (1901–2016), a remotesensing data-driven product (text S2), and the *in situ* observational carbon fluxes (text S3) are available. We use the spun-up surface conditions (i.e. with spun-up surface carbon and nitrogen pools) provided by NCAR to initialize the model. The model runs are summarized in table 1.

2.2. Model benchmarking

2.2.1. Regional GPP and NEE flux estimates

We evaluate CLM using an optimized set of carbon fluxes from the Polar Vegetation Photosynthesis and Respiration Model (PVPRM) during 2012-2014. PVPRM is a functional representation of ecosystem GPP and net ecosystem exchange (NEE) constrained by satellite and tower observations. GPP constraints include: (1) parameter optimization against eddy covariance data for seven arctic and boreal vegetation classes (table S4; Luus and Lin 2015), (2) seasonal phenology as prescribed using solar induced fluorescence (SIF) data from the Global Ozone Monitoring Experiment-2 (GOME-2) satellite with screening for clouds, low sun angles and high albedo surfaces (Joiner et al 2013, Luus et al 2017a, Parazoo et al 2018), and (3) environmental effects using air temperature, soil temperature, and downward shortwave radiation from the North American Regional Reanalysis (NARR; Mesinger et al 2006). This PVPRM based and further constrained GPP product (herein PVPRM-SIF GPP) is validated against eddy covariance data and shows high consistency (Parazoo et al 2018).

The constraint (1) above is also used to constrain ecosystem respiration (ER) from PVPRM, and the constrained ER is used together with the PVPRM-SIF GPP to obtain NEE. This NEE is further optimized using the Weather Research and Forecasting-Stochastic Time-Inverted Lagrangian Transport framework (Lin et al 2003) and atmospheric CO₂ vertical profiles obtained in the lower atmosphere across Alaska from April to November during Carbon in Arctic Reservoirs Vulnerability Experiment (CARVE) campaigns (2012–2014; Chang et al 2014, Commane et al 2017). This NEE product, referred to as CARVE-OPT NEE, show agreement with eddy covariance tower observations (Luus and Lin 2017b) and CRV (CARVE) tower CO₂ flux (Commane et al 2017) in seasonal timing and magnitude for tundra ecosystems (text S2).

The validations of PVPRM-SIF GPP and CARVE-OPT NEE provide confidence in our ability to benchmark CLM carbon dynamics in deciduous ecosystems. We evaluate CLM regional simulations during 2012–2014, and more detailed information on these two datasets is in text S2.

2.2.2. Surface vegetation classes over Alaska

PVPRM surface vegetation distribution are determined by the tree, shrub, and tundra classes over Alaska with the mean cover fractions 25%, 16%, and 44%, respectively; deciduous trees represent a very small percentage (1%) of Alaskan vegetation cover (table S4). PVPRM uses seven vegetation classes over Alaska (table S4), while CLM uses five PFTs (table S2). The primary difference between PVPRM class and CLM PFT maps is that the dominant vegetation in North Slope Alaska (68 °N and north) is described as tundra by PVPRM and represented as a combination of shrub and C3 arctic grass in CLM PFT (figures 2(a) and S1).

To evaluate if CLM can reasonably simulate the vegetation phenology over Alaska, we carry our analysis over three vegetation groups by using the vegetation class map from PVPRM (figure 2). According to the bulk freeze/thaw status of the Alaskan land surface (text S4), the landscape thawing day of North Slope Alaska is typically ∼10–30 d later than that of southern Alaska (figure S3). Thus, we classify the vegetation class in North Slope Alaska as Alaskan northern tundra, separating it from southern Alaskan tundra (figure 2(a)). We combine the southern regions covered by either shrub or by shrub tundra (table S4) into Alaskan shrub (figure 2(b)). According to both PVPRM and CLM, deciduous boreal forest represents a small fraction of Alaskan land cover. Considering the large model grid size $(0.9^{\circ} \text{ latitude} \times 1.25^{\circ} \text{ longitude})$, deciduous boreal forest cannot be studied separately from CLM grid cells. Thus, we treat the three forest classes (table S4) as a single vegetation group, named as Alaskan forest (figure 2(c)). We identify one dominant vegetation group in each PVPRM and CLM grid cell. Vegetation is considered dominant when one of the three vegetation cover fractions exceeds 50% within a grid cell. Overall, our analyses are carried out separately over Alaskan northern tundra, Alaskan shrub, and Alaskan forest.

2.2.3. The definition of budburst start and GPP onset In the default CLM, carbon stored in storage pools will be transferred to the display pools (e.g. leaf carbon pool) when GDD exceeds the GDD threshold (i.e. phenology onset). Leaf carbon is a function of LAI, and the phenology onset triggers the start of LAI accumulation (Oleson et al 2013). At this stage, the model simulates small GPP values and slow GPP growth in the Arctic, since the low temperature slows the vegetation growth. Thus, we define the leaf budburst date as the mean day of year (DOY) when GPP is



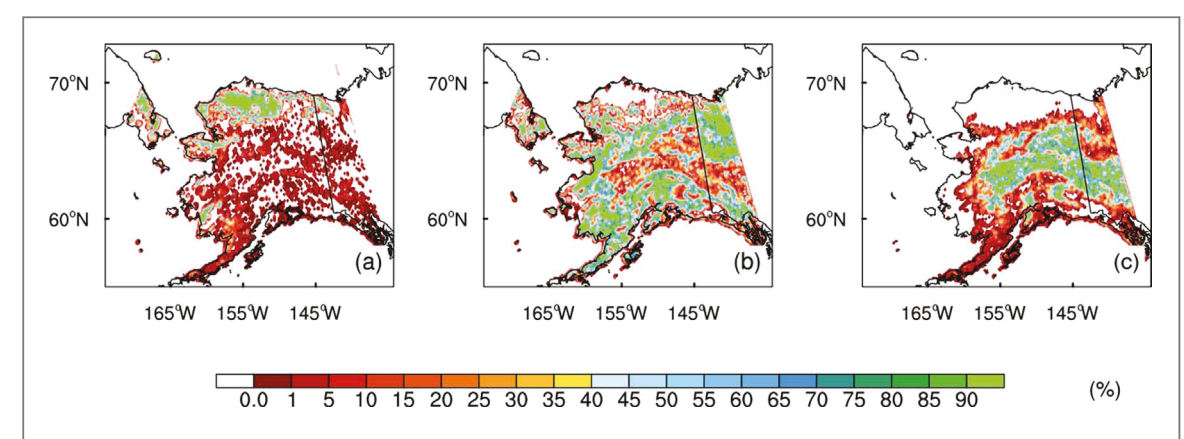


Figure 2. PVPRM prescribed surface vegetation cover fraction over (a) Alaskan northern tundra, (b) Alaskan shrub, and (c) Alaskan forest.

Table 2. DOY of leaf budburst and GPP onset over Alaskan northern tundra, shrub, and forest from PVPRM-SIF, and the DOY differences between PVPRM-SIF and CLM based experiments (i.e. CLM, CLM_GCexp1, CLM_GCexp2, and CLM_GCexp3; model simulations minus PVPRM-SIF). RMSE represents root mean square error.

	PVPRM-	SIF	CLM		CLM_GC	expl	CLM_GC	exp2	CLM_GC	exp3
	Bud-burst	GPP	Bud-burst	GPP	Bud-burst	GPP	Bud-burst	GPP	Bud-burst	GPP
				Alasl	kan northern tur	ıdra				
2012	143	154	3	-2	9	1	16	9	9	3
2013	146	153	5	2	7	4	18	13	8	6
2014	151*	160	-4	-9	8	2	18	11	9	4
					Alaskan shrub					
2012	137	141	-9	-1	-9	4	-9	4	-9	4
2013	143*	145	-11	1	-11	3	-11	2	-11	2
2014	131	145	-10	-12	-9	1	-9	5	-9	2
					Alaskan forest					
2012	131	138	-2	-2	-2	0	0	-2	-2	0
2013	137*	143	-4	0	-5	0	0	-5	-4	0
2014	122	132	0	-1	0	0	0	0	0	0
RMSE	_	_	5.7	4.7	7.8	1.7	12.2	5.1	8.1	2.6

^{*}indicates $D_{\text{BUDBURST, LAST}}$ for each ecosystem.

between 1% and 10% of the peak value of annual GPP (i.e. GPP_{MAX} ; figure 1).

We also define the GPP onset date as the mean DOY when GPP is between 10% and 20% of GPP_{MAX} for that year (Parazoo *et al* 2018). This definition can account for observation noise and range of transition dates from slow to rapid spring recovery in arctic tundra and boreal ecosystems. The number of days between GPP onset and GPP_{MAX} is defined as growth season length. Both the definitions of leaf budburst and GPP onset are tested by using site observations at Imnavait Creek watershed (68.4 °N, 149.2 °W; Euskirchen *et al* 2016; text S5).

2.2.4. PVPRM-SIF inferred Alaskan GPP onset

We investigate how the factors in equation (4) affect dates of leaf budburst for each vegetation group. We first define a 'latest day of budburst', denoted as $D_{\text{BUDBURST, LAST}}$ (table 2), by searching for latest leaf budburst dates in PVPRM-SIF over the period 2012–2014 for each vegetation group. We then use T_{AIR} from NCEP NARR, the meteorological forcing

used to obtain PVPRM-SIF GPP, and the parameter values of exp1 to calculate NCD (number of chill days), $T_{\rm Jan-Feb}$ (the mean $T_{\rm AIR}$ in January and February), GC threshold (values of the right side of equation (4)), and GDDs for all days from 1 January to $D_{\rm BUDBURST,\ LAST}$ in each Alaskan vegetation group (table S5). These calculations are used to investigate how the factors in equation (4) affect PVPRM-SIF GPP suggested DOY of leaf budburst in the three Alaskan vegetation groups.

3. Results

3.1. CLM simulated Alaskan GPP onset

We first investigate if leaf budburst is regulated by $T_{\text{Jan-Feb}}$ and NCD by using PVPRM-SIF GPP and NARR T_{AIR} (equation (4)). Based on section 2.3.4, we find that GDD and chilling exposure can explain the timing of leaf budburst in Alaskan northern tundra and Alaskan shrub (text S6). Since T_{AIR} is the primary factor regulating leaf budburst and GPP onset in highlatitude regions (Euskirchen *et al* 2014), we compare



the $T_{\rm AIR}$ anomalies from CRUNCEP7 with that from NARR during March, April, May, and June over Alaskan northern tundra, shrub, and forest to justify our use of CRUNCEP7. The results suggest that the interannual variability of CRUNCEP7 $T_{\rm AIR}$ matches that of NARR $T_{\rm AIR}$, and it is suitable to study the variability of leaf budburst and GPP onset in CLM driven by CRUNCEP7 (text S7 and figures S4 and S5).

We then use PVPRM-SIF to benchmark CLM estimated GPP onset during 2012-2014. CLM suggested mean DOY of GPP onset are 3, 4, and 1 d earlier than that suggested by PVPRM-SIF in Alaskan northern tundra, shrub, and forest, respectively. Compared to PVPRM-SIF, CLM suggests early DOY of GPP onset ranges from 1 to 12 d across the three vegetation groups (table 2). The spatial difference of GPP onset between CLM and PVPRM-SIF (CLM minus PVPRM-SIF) also shows that CLM suggests ~38% of Alaska has earlier DOY of GPP onset (figure S6). By calculating the root mean square error (RMSE) of the differences between PVPRM-SIF and CLM simulated GPP, we find that CLM_GCexp1 simulated GPP onset has the least divergence (RMSE = 1.7) from that of PVPRM-SIF among all the CLM simulations (table 2). Thus, CLM_GCexp1 gives a best estimation of DOY of GPP onset in the three ecosystems. CLM_GCexp1 postpones the DOY of GPP onset by 5 ± 8 , 6 ± 8 , 1 ± 6 d compared to CLM and reduces the areas with early GPP onset to ~29% of Alaska.

We further study the impacts of the GC model on DOY of GPP onset in the three Alaskan vegetation groups. In Alaskan northern tundra, CLM GPP onset is 2-9 d earlier than in PVPRM-SIF GPP, with the largest difference (i.e. 9 d) in 2014 (table 2). By integrating the GC model with different parameter groups (table S1) into CLM, GPP onset is postponed by a range of 2-20 d over the span of experiments and years. Even though 2014 has the warmest March, April and May (MAM) in Alaskan northern tundra, the delayed GPP onsets are best simulated by CLM_GCexp1 (i.e. 2 d later than the GPP onset of PVPRM-SIF) in 2014. Among the three parameter experiments, CLM_GCexp1 has the best representation of GPP onset compared to PVPRM-SIF, with delays ranging from 1 to 4 d (table 2). In Alaskan shrub, CLM GPP onset is 1 d earlier in 2012, 1 d later in 2013, and 12 days earlier in 2014 than in PVPRM-SIF. This result suggests that without including the GC model, CLM GPP onset diverges from that of PVPRM-SIF during the warm MAM of 2014. Compared to CLM, CLM_GCexp1 gives an improved estimation of GPP onset in Alaskan shrub; in particular, GPP onset is postponed by 13 d in 2014, which is much closer to PVPRM-SIF (table 2). Thus, the GC model also improved the GPP phenology over Alaskan shrub, especially in the years with warmer MAM T_{AIR} (figures S4(b) and (e)). The GPP onset difference between PVPRM-SIF and CLM simulation in Alaskan forest is less than 2 d during 2012–2014 (table 2). In

CLM, needleleaf evergreen boreal trees uses an evergreen phenology model, in which the leaf phenology depends on leaf longevity. Due to the large cover fraction of needleleaf evergreen boreal trees in the surface PFT map of CLM (figures S1(a) and (b), table S2), CLM_GC does not show much sensitivity of GPP onset to the chilling requirement. CLM_GCexp1 can exactly represent GPP onset dates in these three years over Alaskan forest. We also include site-level comparisons based on the measurements of three tundra types at one tundra site and one forest site in Alaska. The comparisons show that CLM simulates earlier GPP onset at both the tundra and forest sites, and the GC model postpones the GPP onset at arctic tundra sites (text S3).

The GC model is also crucial to the growth season length of Alaskan vegetated regions. During 2007–2016, CLM simulated mean DOY of GPP onset is 150 \pm 4, 138 \pm 4, and 134 \pm 5 in Alaskan northern tundra, shrub, and forest, respectively, and the growth season length for the same three ecosystems is 41 ± 6 , 32 ± 10 , and 34 ± 7 d. CLM_GCexp1 postpones the mean DOY of GPP onset to 155 \pm 3, 142 \pm 4, and 135 \pm 4, and shortens the growth season length by 12%, 13%, and 4% in these three ecosystems (figure 3). During 2008–2016, the DOY of GPP onset at the Imnavait Creek watershed (text S3) is 156 \pm 5, 146 \pm 3, and 158 \pm 5 as suggested by the site measurements, CLM, and CLM_GCexp1, respectively. CLM_GCexp1 reduces CLM simulated growth season length (35 d) by 35%. The DOY of leaf budburst has the similar variability (i.e. standard deviation) values to the DOY of GPP onset (figure not shown). Further, these variability numbers of CLM and CLM_GCexp1 show that CLM_GCexp1 only slightly alters GPP onset variability, and the DOY of GPP onset map affirmed this conclusion (figure 4). Additionally, the spatial variability of DOY of GPP onset indicates that Alaskan northern tundra has smaller variability than other Alaskan vegetated regions. Since CRUNCEP7 T_{AIR} always shows a larger variability in Alaskan northern tundra than in other Alaskan regions in April, May and June (AMJ; figure not shown), we infer that Alaskan shrub and forest (mixed with broadleaf deciduous tree, broadleaf deciduous shrub, and C3 arctic grass) have a larger sensitivity to T_{AIR} variations than Alaskan northern tundra (dominated by broadleaf deciduous shrub) as suggested by CLM. The physiological reason for this difference is beyond the scope of this study.

3.2. The GC model induced carbon flux changes in Alaskan spring

Besides GPP phenology, the AMJ carbon fluxes are also affected by the GC model (Jeong *et al* 2012). Thus, we quantify the impacts of the GC model on AMJ carbon flux simulations. According to section 3.1, CLM_GCexp1 has a best estimation of GPP onset in all



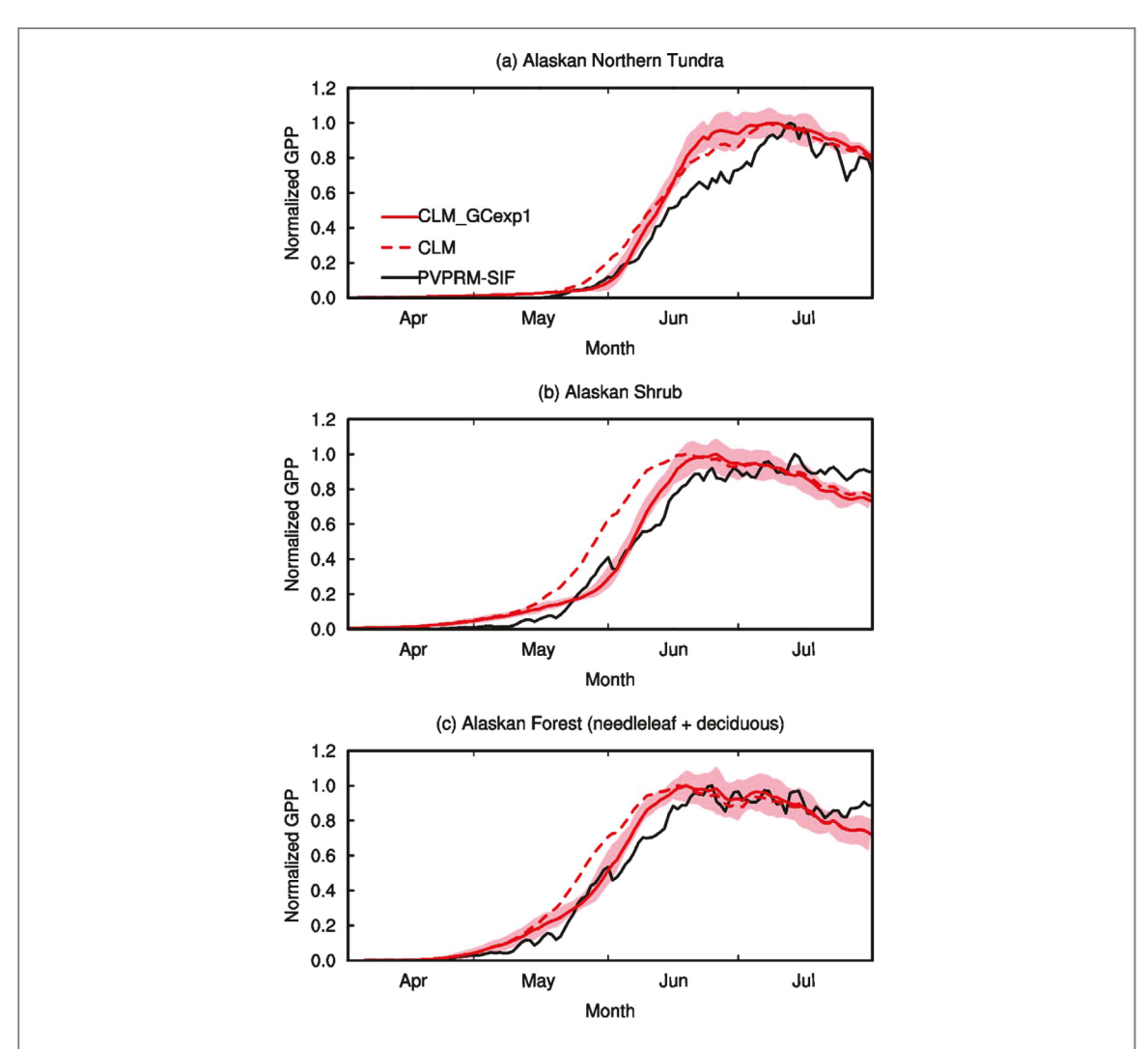


Figure 3. PVPRM-SIF (2012–2014), CLM, and CLM_GCexp1 simulated 2007–2016 mean GPP in April, May, and June (AMJ) over (a) Alaskan northern tundra, (b) Alaskan shrub, and (c) Alaskan forest. All the GPP values are normalized.

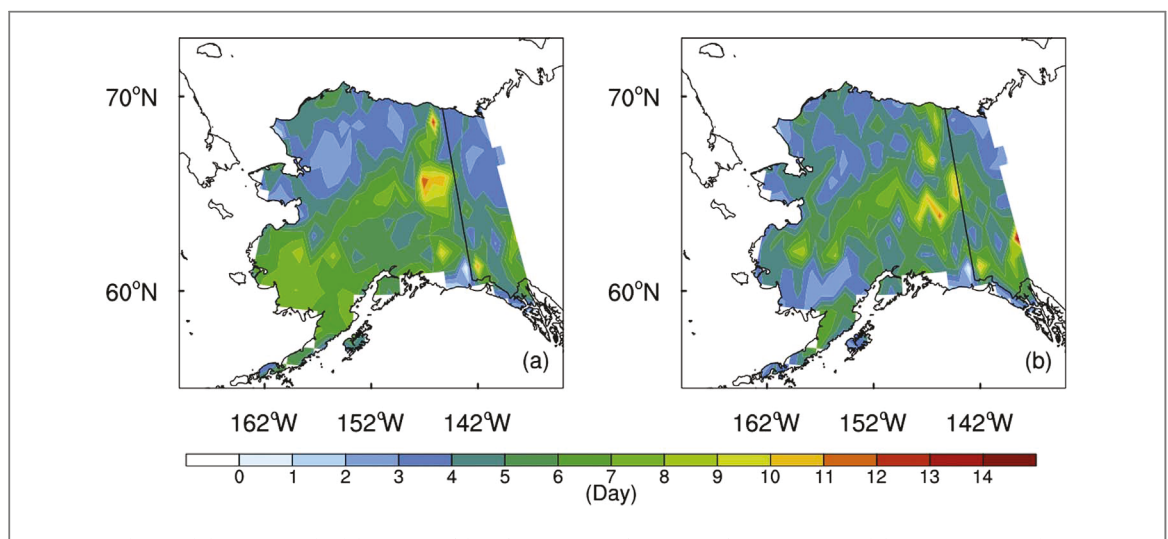


Figure 4. The variability (i.e. standard deviation) of day of year (DOY) of GPP onset from (a) CLM and (b) CLM_GCexp1 during 2007–2016 over Alaska.

the three Alaskan vegetation groups with respect to PVPRM-SIF. Thus, we further study the impacts of CLM_GCexp1 on AMJ GPP and net ecosystem production (NEP; negative value of NEE) during 2012–2014.

In Alaskan northern tundra, AMJ GPP is 0.4 and 0.68 g C m $^{-2}$ d $^{-1}$ for PVPRM-SIF and CLM, respectively. By carrying out CLM_GCexp1, AMJ GPP decreases by 0.02 g C m $^{-2}$ d $^{-1}$ (table 3). Likewise, in



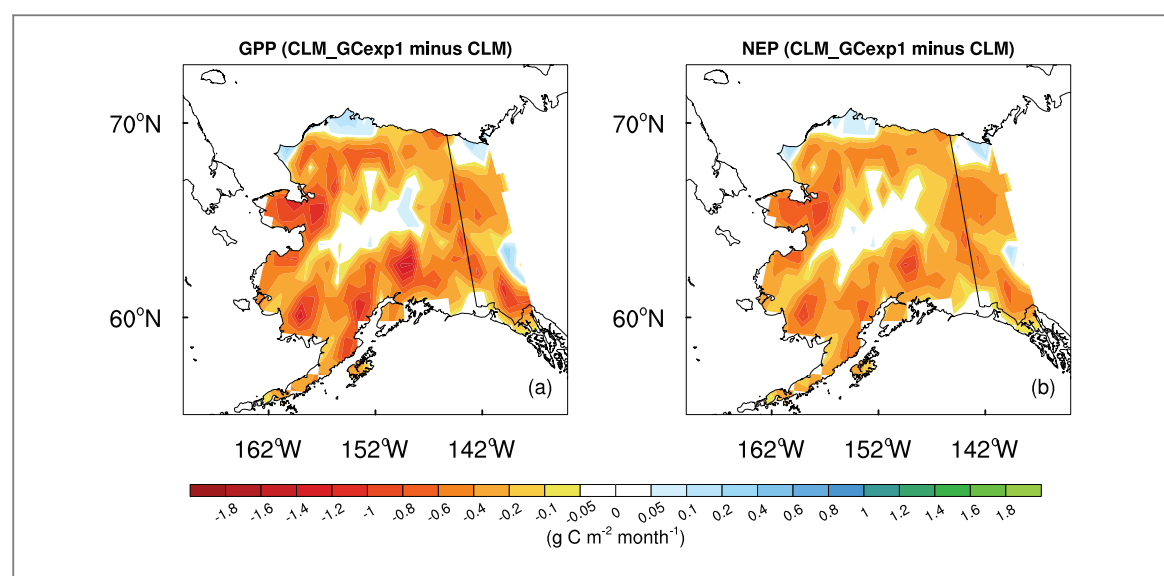


Figure 5. The mean in April, May, and June (AMJ) (a) GPP difference between CLM_GCexp1 and CLM and (b) NEP difference between CLM_GCexp1 and CLM over Alaska during 2012–2014.

Table 3. PVPRM-SIF, CLM, CLM, and GCexp1 suggested 2012–2014 mean AMJ GPP (g C m $^{-2}$ d $^{-1}$) and NEP (g C m $^{-2}$ d $^{-1}$) values over Alaskan northern tundra, Alaskan shrub, and Alaskan forest.

	PVPRM-SIF	CLM	CLM_CGexp1		
	Alaskan no	rthern tund	lra		
GPP	0.40	0.68	0.66		
NEP	-0.47	0.06	0.04		
	Alask	an shrub			
GPP	0.84	2.73	2.34		
NEP	0.17	0.41	0.11		
	Alask	an forest			
GPP	2.17	3.09	2.85		
NEP	0.61	0.59	0.38		
	Three vegetati	on group av	rerage		
GPP	1.11	2.31	2.03		
NEP	0.17	0.38	0.16		

Alaskan shrub, AMJ GPP is 0.84 and 1.89 C m⁻² d⁻¹ for PVPRM-SIF and CLM, respectively, and CLM_GCexp1 leads to a GPP reduction of 0.39 g C $m^{-2} d^{-1}$ (14%) over default CLM (table 3). We find a similar pattern of GPP reduction associated with CLM GCexp1 over Alaskan forest (table 3). Here, CLM overestimates AMJ GPP in all three Alaskan vegetation groups compared to PVPRM-SIF GPP, especially over Alaskan shrub. CLM_GCexp1 simulated GPP fluxes suggest that among the three Alaskan vegetation groups, Alaskan shrub has the largest fraction of AMJ GPP reduction with the value of 14% (table 3). We also investigate AMJ GPP flux over all the Alaskan vegetated region (vegetation cover fraction ≥50%). The results also show that AMJ GPP is overestimated by CLM (by 110%) compared to PVPRM-SIF. CLM_GCexp1 reduces the AMJ GPP by 12% $(0.28 \text{ g C m}^{-2} \text{ d}^{-1}; \text{ figure 5(a)})$. Thus, the GC model could reduce the high AMJ GPP bias in CLM.

We use CARVE-OPT NEP to further benchmark CLM. Integrating CARVE-OPT NEP over all Alaskan

vegetated areas, we find a mean AMJ uptake during 2012-2014 of 0.17 g C m⁻² d⁻¹, indicating a growth season carbon sink. In comparison, the mean AMJ NEP in Alaskan northern tundra, shrub, and forest is $-0.47\,g\,C\,\,m^{-2}\,\,d^{-1}\!,\;0.17\,g\,C\,\,m^{-2}\,\,d^{-1}\!,\;\text{and}\;0.61\,g\,C$ m⁻² d⁻¹, respectively, indicating the Alaskan growth season sink is associated with shrub and forest (table 3). Compared to CARVE-OPT, CLM overestimates net Alaskan AMJ uptake by a factor of two (NEP = $0.38 \text{ g C m}^{-2} \text{ d}^{-1}$), producing sinks in all three vegetation groups (NEP = 0.06, 0.41, and 0.59 g C m⁻² d⁻¹ in northern tundra, shrub, and forest, respectively). CLM_GCexp1 reduces this sink by $0.22 \text{ g C m}^{-2} \text{ d}^{-1}$ (figure 5(b)), in closer agreement with CARVE-OPT. The variations of Alaskan carbon fluxes at the yearly time scale are discussed in Text S8.

4. Discussion

Model intercomparisons have repeatedly shown an early bias in predicted photosynthetic-growing season onset in northern high latitudes on local to regional scales (Richardson et al 2012, Peng et al 2015, Commane et al 2017). Previous studies have hinted that leaf budburst and subsequent GPP onset in temperature limited ecosystems are sensitive to accumulated GDD as well as cold temperature (chilling) exposure. By integrating a new phenology model into CLM that accounts for both effects (CLM_GCexp1), we are able to successfully postpone GPP onset in Alaskan northern tundra and shrub by 5 ± 7 and $4\pm8\,\mathrm{d}$ and reduce spring GPP magnitude by 2.5 g C m^{-2} and 32.1 g C m^{-2} during 2007–2016. These variations lead to a reduction in spring (AMJ) GPP of 10% from 2007 to 2016. Overall, we find CLM_GCexp1 delays GPP onset by 2-13 d compared to the unadjusted CLM over Alaska from 2012 to 2014, closer agreement with an observationally



constrained benchmark (PVPRM). The model simulated GPP in Alaskan forests is not as strongly affected in the new model due to dominance of needleleaf evergreen tree over Alaska. These results suggest that the thermal forcing models with a chilling requirement have the potential of reducing the uncertainty of TBM simulated spring phenology in high-latitude regions.

The timing of leaf budburst is mostly unchanged in CLM_GCexp1, with the exception that leaf budburst in tundra is further delayed relative to PVPRM-SIF from 1 d in CLM to 8 d in CLM_GCexp1 over 2012–2014 (table 2). We note a couple caveats here. First is the transition to spring green-up is very slow and noisy from PVPRM (and *in situ* observations), making detection of a ~5% threshold for leaf budburst uncertain. Second is that PVPRM-SIF uncertainty increases moving into earlier spring with reduced signal and increased noise in the spaceborne SIF constraint. As such, further testing of budburst in Alaskan deciduous vegetation types is needed.

The new model also alters the structure of peak growing season GPP. Specifically, CLM_GCexp1 shifts the timing of peak GPP by -6, 7, 3 d and amplifies the magnitude of peak GPP by 4.7%, 0.9%, and 9.2% over Alaskan northern tundra, shrub, and forest, respectively, during 2007–2016 (figure 3; 3.6% increase on average). It is likely that the increase of annual GPP peak could be associated with a postponed leaf budburst, which might allow more nitrogen accumulation in soil during and after soil thaw and then trigger a higher GPP amount after GPP onset (Larsen *et al* 2007, text S8).

To improve the consistency of annual maximum LAI values between MODIS and CLM, CESM Version 2 (CESM2.0) updates its high-latitude PFT map, producing a 26% increase in C3 arctic grass fraction in Alaska (table S2). CLM simulations based on this updated PFT map (herein CLM_P2) produce larger disagreement in GPP phenology (raised early bias) and magnitude (increased high bias) over Alaskan northern tundra and Alaskan shrub compared to simulations with the original map (table S5). These results and the improved vegetation map used by CLM_P2 imply that the functionality rather than the surface misrepresentation of PFTs induces the overestimated GPP in CLM. Thus, uncertainties still exist in GPP simulations in the photosynthetic module of CLM and other TBMs. Future studies at smaller spatial scales (i.e. Alaskan tower sites) are needed to identify the reasons, which could be associated with photosynthetic related prognostic variables (e.g. Vcmax) and nutrient limitations (Rogers et al 2019).

Parameter availability limits the application of the GC model to different PFTs in arctic tundra and boreal ecosystems over Alaska. We test all the parameters obtained from temperate forest observations in Jeong *et al* (2012) and (2013) and select the parameter groups that can be reasonably applied into CLM over Alaska.

All the three experiments, using the same model structure (equations (3) and (4)) but different parameter groups (table S1), show the sensitivity of 'GDD plus chilling requirement' to different parameter groups. Here, we find that with the same number of NCD, exp2 provides higher GC threshold values than exp1 (figure S7). Thus, exp2 requires a higher number of GDD suggested in equation (3), which takes a longer accumulative time period, to trigger the leaf budburst. This structure of the GC model explains the later GPP onset represented by exp2 than by exp1 (table 3). We also try to use the least-square curve-fitting method and the observations at the Imnavait Creek watershed to optimize the parameters. However, owing to the limited amount of data, the result does not coverage. Thus, acquiring and synthesizing more budburst records over the Arctic (Euskirchen et al 2014) and using varied approaches for parameter optimization are needed for carbon cycle studies and for the potential improvements to GPP phenology representation in CMIP models (Anav et al 2013) in high-latitude regions.

The existing studies on climate change and plant phenology in Arctic tundra are very limited compared to similar studies in lower latitudes (Diepstraten et al 2018). Additionally, the range of chilling temperatures needed for ending dormancy has not yet been identified for different Arctic deciduous vegetation types (Dantec et al 2014). This limitation is associated with the complexity of understanding the biological processes and the high cost in maintaining long-term observations to understand how these biological processes are affected by the changing environmental factors in Arctic tundra (Diepstraten et al 2018). Bjorkman et al (2015) show that the timing of snowmelt is also a strong driver of flowering phenology, especially for early-flowering species over Arctic tundra, while the flowering phenology for late-flowering species depends on spring temperature. With the observational limitations, disentangling the impacts of different environmental factors on plant phenology and including these impacts into phenology representations of TBMs are still a challenge with respect to improving phenology simulations over Arctic ecosystems. Thus, high spatial and temporal resolution observations that can monitor vegetation phenology are needed to be advanced for carbon cycle studies in high-latitude regions.

5. Conclusions

We integrated a model which includes GDDs and a new chilling requirement into CLM. Compared to a model constrained by satellite observations (PVPRM-SIF), we find the chilling requirement can better represent photosynthetic onset in Alaskan deciduous vegetated regions. The revised model postpones photosynthetic onset over Alaskan northern tundra



and shrub by 2–13 d over the period 2012–2014, with greatest improvement during warm springs (e.g. 2014). Our GC model also reduces the high AMJ GPP bias (compared PVPRM-SIF GPP) by ~12% over vegetated Alaskan areas. Investigation of additional processes such as nitrogen limitation is needed to further reduce high GPP bias in CLM. This study represents a critical step forward in predicting Arctic deciduous vegetation phenology and its response to future warming.

Acknowledgments

Support from the NASA Earth Science Division Interdisciplinary Science program (16-IDS16-0072) and the Terrestrial Ecology program's Arctic Boreal Vulnerability Experiment (ABoVE) are acknowledged. We appreciate Dr Hideki Kobayashi and Professor Ueyama Masahito in providing valuable suggestions on site-level observations. The US-Prr site (Poker Flat Research Range) is supported by JAMSTEC and IARC/UAF collaboration study (JICS) and Arctic Challenge for Sustainability Project (ArCS). MS, NCP, and CEM carried out the research at the Jet Propulsion Laboratory, California Institute of Technology, under a contract with NASA. MS also carried out the research at the Joint Institute for Regional Earth System Science and Engineering, University of California at Los Angeles. S-J J was supported by the National Research Foundation of Korea (NRF) grant funded by the Korea government (MSIT) (NRF-2019R1A2C3002868). 2019. All rights reserved.

Data Availability Statements

The CARVE-OPT NEE that supports the findings of this research is available at https://daac.ornl.gov/cgi-bin/ dsviewer.pl?ds_id=1389 (DOI:10.3334/ORNLDAAC/ 1389). PVPRM-SIF GPP that supports the findings of this research is available at https://daac.ornl. gov/cgi-bin/dsviewer.pl?ds_id=1314 (DOI: 10.3334/ ORNLDAAC/1314). The Advanced Microwave Scanning Radiometer (AMSR-E) and the Special Sensor Microwave Imager (SSM/I) soil freeze/thaw data are at https://nsidc.org/data/NSIDC-0477/versions/3 (DOI: 10.5067/MEASURES/CRYOSPHERE/nsidc-0477.003). The measurements at Brooks Range in the Imnavait Creek watershed are available at http://aon. iab.uaf.edu/data access (DOI:10.1007/s10021-016-0085-9). The measurements at Poker Flat Research Range are available at https://ameriflux.lbl.gov/sites/ siteinfo/US-Prr (DOI:10.17190/AMF/1246153). The atmospheric forcing data of Climatic Research Unit-National Centers for Environmental Prediction Version 7 (CRUNCEP7) are presented in Lawrence et al (2019) (DOI:10.1029/2018MS001583), and available https://rda.ucar.edu/datasets/ds314.3/. The North American Regional Reanalysis (NARR) is presented in

Mesinger *et al* (2006) (DOI:10.1175/BAMS-87-3-343) and available at https://ncdc.noaa.gov/data-access/model-data/model-datasets/north-american-regional-reanalysis-narr. CLM4.5 is available at the repository of NCAR, and the updated model code including the GC model are available from the corresponding author upon request.

ORCID iDs

2469-4831
Nicholas C Parazoo https://orcid.org/0000-0002-4424-7780
Su-Jong Jeong https://orcid.org/0000-0003-4586-4534
Leah Birch https://orcid.org/0000-0002-0371-109X
Peter Lawrence https://orcid.org/0000-0002-4843-4903
Eugenie S Euskirchen https://orcid.org/0000-0002-0848-4295
Charles E Miller https://orcid.org/0000-0002-

Mingjie Shi https://orcid.org/0000-0002-

References

9380-4838

Anav A, Friedlingstein P, Kidston M, Bopp L, Ciais P, Cox P, Jones C, Jung M, Myneni R and Zhu Z 2013 Evaluating the land and ocean components of the global carbon cycle in the CMIP5 earth system models *J. Clim.* 26 6801–43

Baldocchi D and Wong S 2008 Accumulated winter chill is decreasing in the fruit growing regions of California *Clim. Change* 87 153–66

Beck P S A, Horning N, Goetz S J, Loranty M M and Tape K D 2011 Shrub Cover on the north slope of Alaska: a circa 2000 baseline map *Arctic Antarctic Alpine Res.* 43 355–63

Berner L T, Jantz P, Tape K D and Goetz S 2018 Tundra plant aboveground biomass and shrub dominance mapped across the north slope of Alaska *Environ. Res. Lett.* 13 035002

Bjorkman A D, Elmendorf S C, Beamish A L, Vellend M and Henry G H R 2015 Contrasting effects of warming and increased snowfall on Arctic tundra plant phenology over the past two decades *Glob. Change Biol.* 21 4651–61

Bonan G B 2008 Forests and climate change: forcings, feedbacks, and the climate benefits of forests *Science* 320 1444–9

Caffarra A, Donnelly A, Chuine I and Jones MB 2011 Modelling the timing of Betula pubescens budburst. I. Temperature and photoperiod: a conceptual model *Clim. Res.* 46 147–57

Chang R Y *et al* 2014 Methane emissions from Alaska in 2012 from CARVE airborne observations *Proc. Natl Acad. Sci.* 111 16694–9

Chiang J M and Brown K J 2007 Improving the budburst phenology subroutine in the forest carbon model PnET *Ecol. Modelling* 205 515–26

Clark James S, Salk Carl, Melillo Jerry and Mohan Jacqueline 2014

Tree phenology responses to winter chilling, spring warming, at north and south range limits Funct. Ecol. 28 1344–55

Commane R et al 2017 Carbon dioxide sources from Alaska driven by increasing early winter respiration from Arctic tundra Proc. Natl Acad. Sci. 114 5361–6

Dantec C F, Vitasse Y, Bonhomme M, Louvet J M, Kremer A and Delzon S 2014 Chilling and heat requirements for leaf unfolding in European beech and sessile oak populations at the southern limit of their distribution range *Int. J. Biometeorol.* **58** 1853–64



- Delbart N and Picard G 2007 Modeling the date of leaf appearance in low-arctic tundra *Glob. Change Biol.* 13 2551–62
- Delpierre Nicolas, Vitasse Yann, Chuine Isabelle, Guillemot Joannès, Bazot Stéphane, Rutishauser This and Rathgeber Cyrille B. K. 2016 Temperate and boreal forest tree phenology: from organ-scale processes to terrestrial ecosystem models *Annals of Forest Science* 73 5–25
- Diepstraten R A, Jessen T D, Fauvelle M D and Musiani M M 2018 Does climate change and plant phenology research neglect the Arctic tundra? *Ecosphere* 9 e02362
- Euskirchen E S *et al* 2006 Importance of recent shifts in soil thermal dynamics on growing season length, productivity, and carbon sequestration in terrestrial high-latitude ecosystems *Glob*. *Change Biol.* 12731–50
- Euskirchen E S, Carman T B and Mcguire A D 2014 Changes in the structure and function of northern Alaskan ecosystems when considering variable leaf-out times across groupings of species in a dynamic vegetation model *Glob. Change Biol.* 20
- Euskirchen E. S., Bret-Harte M. S., Shaver G. R., Edgar C. W. and Romanovsky V. E. 2016 Long-Term Release of Carbon Dioxide from Arctic Tundra Ecosystems in Alaska *Ecosystems*
- El Maayar M, Price D T, Black T A, Humphreys E R and Jork E M 2002 Sensitivity tests of the integrated biosphere simulator to soil and vegetation characteristics in a Pacific coastal coniferous forest *Atmos. Ocean* 40 313–32
- Jeong S J, Ho C H, Gim H J and Brown M E 2011 Phenology shifts at start vs. end of growing season in temperate vegetation over the Northern Hemisphere for the period 1982–2008 *Glob*. *Change Biol*. 17 2385–99
- Jeong S J, Medvigy D, Shevliakova E and Malyshev S 2012 Uncertainties in terrestrial carbon budgets related to spring phenology J. Geophys. Res. Biogeosci. 117 G01030
- Jeong S J, Medvigy D, Shevliakova E and Malyshev S 2013 Predicting changes in temperate forest budburst using continental-scale observations and models *Geophys. Res.* Lett. 40 359–64
- Joiner J, Guanter L, Lindstrot R, Voigt M, Vasilkov A P, Middleton E M, Huemmrich K F, Yoshida Y and Frankenberg C 2013 Global monitoring of terrestrial chlorophyll fluorescence from moderate-spectral-resolution near-infrared satellite measurements: methodology, simulations, and application to GOME-2 Atmos. Meas. Tech. 6 2803–23
- Krinner G, Viovy N, de Noblet-Ducoudré N, Ogée J, Polcher J, Friedlingstein P, Ciais P, Sitch S and Prentice I. C 2005 A dynamic global vegetation model for studies of the coupled atmosphere-biosphere system *Global Biogeochem*. Cycles 19
- Larsen K S, Grogan P, Jonasson S and Michelsen A 2007 Respiration and microbial dynamics in two subarctic ecosystems during winter and spring thaw: effects of increased snow depth *Arctic Antarctic Alpine Res.* 39 268–76
- Laube J, Sparks T H, Estrella N, Hofler J, Ankerst D P and Menzel A 2014 Chilling outweighs photoperiod in preventing precocious spring development *Glob. Change Biol.* 20 170–82
- Lawrence D M et al 2019 Parameterization improvements and functional and structural advances in Version 4 of the community land model J. Adv. Modeling Earth Syst. 3 M03001
- Lawrence P J and Chase T N 2007 Representing a new MODIS consistent land surface in the community land model (CLM 3.0) J. Geophys. Res. 112 G01023
- Levis S and Bonan G B 2004 Simulating springtime temperature patterns in the community atmosphere model coupled to the community land model using prognostic leaf area *J. Clim.* 17 4531–40
- Lin J C, Gerbig C, Wofsy S C, Andrews A E, Daube B C, Davis K J and Granger C A 2003 A near-field tool for simulating the upstream influence of atmospheric observations: The Stochastic Time-Inverted Lagrangian Transport (STILT) model Journal of Geophysical Research 108 4493

- Luus K A *et al* 2017a Tundra photosynthesis captured by satelliteobserved solar-induced chlorophyll fluorescence *Geophys*. *Res. Lett.* 44 1564–73
- Luus K A and Lin J C 2015 The polar vegetation photosynthesis and respiration model: a parsimonious, satellite-data-driven model of high-latitude ${\rm CO_2}$ exchange Geosci. Model Dev. 8 2655–74
- Luus K A and Lin J C 2017b CARVE Modeled Gross Ecosystem CO₂
 Exchange and Respiration, Alaska, 2012–2014 (Oak Ridge,
 Tennessee: ORNL DAAC) (https://doi.org/10.3334/
 ORNLDAAC/1314)
- Melaas E K, Sulla-Menashe D and Friedl M A 2018 Multidecadal changes and interannual variation in springtime phenology of north american temperate and boreal deciduous forests *Geophys. Res. Lett.* 45 2679–87
- Mesinger F et al 2006 North american region reanalysis Bull. Am. Meteorol. Soc. 87 343–60
- Myneni R B, Keeling C D, Tucker C J, Asrar G and Nemani R R 1997 Increased plant growth in the northern high latitudes from 1981 to 1991 *Nature* 386 698
- Oleson K et al 2013 Technical description of version 4.5 of the Community Land Model (CLM) Technical Note No. NCAR/ TN-503+STR (Boulder, CO: National Center for Atmospheric Research) (https://doi.org/10.5065/D6RR1W7M)
- Parazoo N C et al 2018 Spring photosynthetic onset and net CO_2 uptake in Alaska triggered by landscape thawing Glob. Change Biol. 24 3416–35
- Peng S et al 2015 Benchmarking the seasonal cycle of CO_2 fluxes simulated by terrestrial ecosystem models Glob. Biogeochem. Cycles 29 46–64
- Piao S et al 2013 Evaluation of terrestrial carbon cycle models for their response to climate variability and to ${\rm CO_2}$ trends Glob. Change Biol. 19 2117–32
- Piao S, Friedlingstein P, Ciais P, Viovy N and Demarty J 2007 Growing season extension and its impact on terrestrial carbon cycle in the Northern Hemisphere over the past 2 decades *Glob. Biogeochem. Cycles* 21 GB3018
- Randerson JT, Field CB, Fung IY and Tans PP 1999 Increases in early season ecosystem uptake explain recent changes in the seasonal cycle of atmospheric CO_2 at high northern latitudes *Geophys. Res. Lett.* 26 2765–8
- Richardson A D et al 2012 Terrestrial biosphere models need better representation of vegetation phenology: results from the North America carbon program site synthesis Glob. Change Biol. 8 566–84
- Richardson A D and O'Keefe J 2009 Phenological differences between understory and overstory: a case study using the long-term harvard forest records *Phenology of Ecosystem Processes* ed A Noormets (New York: Springer) pp 87–117
- Rogers A, Serbin S P, Ely K S and Wullschleger S D 2019 Terrestrial biosphere models may overestimate Arctic CO 2 assimilation if they do not account for decreased quantum yield and convexity at low temperature *New Phytologist* 223 167–79
- Schaefer K, Denning AS and Leonard O 2005 The winter Arctic Oscillation, the timing of spring, and carbon fluxes in the Northern Hemisphere Glob. Biogeochem. Cycles 19 GB3017
- Schwartz M D and Hanes J M 2010 Continental-scale phenology: warming and chilling *Int. J. Climatol.* **30** 1595–8
- Screen J A and Simmonds I 2010 The central role of diminishing sea ice in recent Arctic temperature amplification *Nature* 464 1334
- Screen J A, Simmonds I, Deser C and Tomas R 2013 The atmospheric response to three decades of observed Arctic sea ice loss *J. Clim.* **26** 1230–48
- Serreze M, Barrett A, Stroeve J, Kindig D and Holland M 2009 The emergence of surface-based Arctic amplification *Cryosphere* 3 11
- Sitch S *et al* 2003 Evaluation of ecosystem dynamics, plant geography and terrestrial carbon cycling in the LPJ dynamic global vegetation model *Glob. Change Biol.* **9** 161–85
- Sitch S $\it et\,al\,2008$ Evaluation of the terrestrial carbon cycle, future plant geography and climate-carbon cycle feedbacks using



five dynamic global vegetation models (DGVMs) *Glob. Change Biol.* **14** 2015–39

Thornton P E *et al* 2002 Modeling and measuring the effects of disturbance history and climate on carbon and water budgets in evergreen needleleaf forests *Agric. For. Meteorol.* **113** 185–222

White M A, Thornton P E and Running S W 1997 A continental phenology model for monitoring vegetation responses to

interannual climatic variability *Glob. Biogeochem. Cycles* 11 217–34

Wipf S and Rixen C 2010 A review of snow manipulation experiments in Arctic and alpine tundra ecosystems *Polar Res.* 29 95–109

Zeng H, Jia G and Epstein H 2011 Recent changes in phenology over the northern high latitudes detected from multi-satellite data *Environ. Res. Lett.* 6 045508